Journal of Photochemistry and Photobiology A: Chemistry 277 (2014) 75–81

Contents lists available at ScienceDirect

Journal of Photochemistry and Photobiology A: Chemistry

journal homepage: www.elsevier.com/locate/jphotochem

Green-emissive molecular marker with a TRIS-scaffold for fluorescence imaging of Zn^{2+} in biological systems

Sougata Sinha [a], Trinetra Mukherjee [b], Jomon Mathew [c], Subhra Kanti Mukhopadhyay [b,*], Subrata Ghosh [a,**]

[a] School of Basic Sciences, Indian Institute of Technology Mandi, Mandi 175001, H.P., India
[b] Department of Microbiology, Burdwan University, Burdwan, W. B., India
[c] Schulich Faculty of Chemistry and the Lise Meitner Minerva Center for Computational Quantum Chemistry, Technion-Israel Institute of Technology, Haifa, Israel

ARTICLE INFO

Article history:
Received 2 November 2013
Received in revised form 3 December 2013
Accepted 16 December 2013
Available online 21 December 2013

This paper is dedicated to Professor Jean-Paul Lellouche.

Keywords:
Molecular probe
Fluorescence bioimaging
Gram seed sprouts
Intracellular detection
Zinc translocation

ABSTRACT

Three TRIS-based molecular probes, **L1**/**L2**/**L3**, were screened for their ability to detect Zn^{2+} at nanomolar level. Keeping in mind the criteria for a molecular probe to be utilized as bioimaging material, **L2** was chosen as model compound for biological studies due to its higher excitation/emission wavelengths. While investigating the potential of **L2**, intracellular Zn^{2+} was successfully imaged using fluorescence microscopy. As the fluorescence emission of **L2**-Zn^{2+} ensemble was stable for longer duration, more than 3 h, **L2** was successfully utilized in *in vivo* imaging of Zn^{2+} in a whole plant (*Peperomia pellucida*) in real-time. Further to its *in vivo* imaging capability, **L2** was found to be successful in imaging zinc pool of gram seed sprouts.

1. Introduction

Over the years, efforts have been directed to develop various methodologies/techniques to better understand every detail and principle of biological systems. Fluorescence bioimaging is one among them that enabled us to enrich our knowledge in understanding various biological events [1–21]. While biologically abundant metal ions like Na^+, K^+, Ca^{2+} and Mg^{2+} are highly essential for living systems, Zn^{2+} is the second most abundant transition metal in human body [22]. Imaging, both *in vitro* and *in vivo*, of such biologically important metal ions using fluorescence microscopy technique has helped us in furthering our understanding of the cell biology of metal ions. Therefore, it is an ongoing endeavor to develop cell permeable molecular probe for imaging of these metal ions in living systems. Though, both fluorescence turn-on and turn-off mechanisms [4,7,11,13–21,23–27] have been used in the last few decades for the detection of these metal ions inside living systems, turn-on probes are always more desirable. For a molecular probe to be an efficient bioimaging material, the probe should satisfy some of the criteria such as solubility in aqueous/semi-aqueous media, cell permeation capability, bright signaling, less or no background fluorescence, and higher excitation/emission wavelengths [1].

Zinc plays various important roles in different biological processes such as in neurotransmission, apoptosis, gene expression, and DNA/RNA synthesis [28–32]. In addition to these, it regulates the activities of wide range of enzymes [33]. As per the reported data, a normal human body contains up to 3 g of zinc, and the amount varies from nanomolar to milimolar concentration inside other biological systems [34,35]. Though zinc is the second most abundant metal ion and key in monitoring various biological events in human body, its over accumulation inside cells may cause severe damage to human health. Whereas the role of chelated zinc in biological systems is well investigated and documented in the literature, the biological functions of labile/free zinc pool in living system remain unclear. In this regard, small molecule based fluorescence imaging of these zinc pools is providing us with valuable information on various important biological events [1,3,9–11,27,30,34,36–65]. Therefore, development of fluorescence

* Corresponding author.
** Corresponding author. Tel.: +91 1905 237926; fax: +91 1905 237924.
E-mail addresses: skmmicro@gmail.com (S.K. Mukhopadhyay), subrata@iitmandi.ac.in (S. Ghosh).

1010-6030/$ – see front matter © 2013 Elsevier B.V. All rights reserved.
http://dx.doi.org/10.1016/j.jphotochem.2013.12.012

turn-on molecular probes which offer real-time analysis option for *in vivo* studies and with high degree of selectivity for Zn^{2+} over Na^+, K^+, Ca^{2+} and Mg^{2+} is an important and challenging area of research.

The present work demonstrates our recent studies on utilization of TRIS-based molecular probe as Zn^{2+}-specific fluorescence bioimaging material. The *in vitro* zinc imaging potential of the present probe was established using *Bacillus thuringiensis* cell line. The imaging of zinc in a whole plant and in gram sprouts supported the probe's capability as bioimaging material for *in vivo* studies in real-time.

2. Experimental

2.1. Materials

Chemicals and solvents were obtained from commercial sources and used as received. Spectroscopic grade DMF was used to perform all spectroscopy related experiments. The metal salts were used in their nitrate form (except Hg^{2+} and Mn^{2+} which were used as chloride salts). To obtain a fixed pH, 10 mM pH 7.0 HEPES buffer was used as aqueous medium. Quantum yield was calculated using quinine sulfate as reference.

2.2. Instruments

Absorption and emission spectra were recorded on Simadzu UV-2450 and Cary Eclipse fluorescence spectrophotometers respectively at ~25 °C. All spectral studies were performed at 1 cm quartz cell with 5 slit widths for both excitation and emission. FT-IR spectra were recorded on a Perkin Elmer Spectrum 2 spectrophotometer. ^1H and ^{13}C NMR spectra were recorded on Jeol JNM ECX 400 MHz and Bruker Avance 300 MHz spectrometer in DMSO-*d6*. The imaging system was comprised of an inverted fluorescence microscope (Leica DM 1000 LED), digital compact camera (Leica DFC 420C), and an image processor (Leica Application Suite v3.3.0). The microscope was equipped with a mercury 50 W lamp.

2.3. Binding constant calculation

The equation that was used to calculate binding constant is $[G]_{tot} = a/2K_{21}(1-a)^2[H]_{tot} + a[H]_{tot}/2$ [66,67], where $[G]_{tot}$ is total concentration of guest (here Zn^{2+}), $[H]_{tot}$ is the total concentration of host, $a = (A - A_o)/(A_{inf} - A_o)$ where A is the absorbance at a particular Zn^{2+} concentration, A_o and A_{inf} are the absorbances at zero and infinite Zn^{2+} concentrations, respectively.

2.4. Cell culture and intracellular zinc imaging

B. thuringiensis (strain isolated in our laboratory as a biopesticide agent for controlling looper pest of tea and identified on the basis of 16S rDNA gene sequence homology) cells from exponentially growing culture in Nutrient broth (pH 7.2, incubation temperature 29 °C) were collected by centrifugation at 3000 rpm for 5 min. After collection, these two types of cells were washed twice by suspending them in 0.1 M HEPES buffer (pH 7.4) followed by centrifugation in the same speed as above. The washed cells were then treated separately with the zinc salt, $Zn(NO_3)_2{\cdot}6H_2O$ (0.05 mM) for 30 min. After completion of this incubation process the cells were further washed with 0.1 M HEPES buffer (pH 7.4). The washed cells were then further incubated with **L2** (0.05 mM) for another 30 min. Finally, and to minimize background fluorescence, the treated cells were washed further and then mounted on grease free glass slide and observed under a Leica DM 1000 Fluorescence microscope with UV filter. Cells treated with $Zn(NO_3)_2{\cdot}6H_2O$ but not with ligand and cells without $Zn(NO_3)_2{\cdot}6H_2O$ treatment but incubated with ligand were chosen as control.

2.5. Zinc imaging in gram seed sprouts

Matured gram seeds were germinated at room temperature using distilled water. The sprouted seeds were then treated with $Zn(NO_3)_2{\cdot}6H_2O$ solution for 2 h. After completion of zinc incubation, the seeds were washed several times with water to remove surface sticking $Zn(NO_3)_2{\cdot}6H_2O$. Some of these incubated seeds were then further incubated with probe **L2** (0.5 mM) for 1 h. After completion of incubation with probe **L2**, the seeds were thoroughly washed and then sectioned. Finally, the sections were imaged using a fluorescence microscope. Sprout sections treated with $Zn(NO_3)_2{\cdot}6H_2O$ but not with probe **L2** and sections without $Zn(NO_3)_2{\cdot}6H_2O$ treatment but incubated with probe **L2** were used as control.

3. Results and discussion

3.1. Synthesis

Probes **L1/L2/L3** were synthesized using a simple one-pot condensation reaction between tris(hydroxymethyl)aminomethane (TRIS) and various salicylaldehydes in ethanol under refluxing condition (Scheme 1). The products were obtained as yellow/red solids and thoroughly characterized using spectroscopic tools such as FT-IR, NMR and mass spectroscopy. The spectral data of **L1** and **L3** were in agreement with the reported data [68,69].

3.2. UV–vis and fluorescence studies

To study the photo physical properties of ligands **L1/L2/L3**, in the presence and absence of Zn^{2+}, we started with UV–vis titration of **L1**. Three peaks were observed in the absorption spectra of **L1** (2×10^{-5} M) in DMF/Water (9:1) at 280, 317, and 409 nm (Fig. S1). Addition of increasing amount of Zn^{2+} (0–16×10^{-5} M) resulted in generation of a new absorption band centered at 364 nm. After binding with Zn^{2+} the absorption peak at 409 nm almost disappeared and a strong decrease in intensity in absorption band centered at 317 nm was observed. Appearance of two isobestic points at 330 and 398 nm clearly indicated the formation of **L1**-Zn^{2+} complex (Fig. S1). The generation of new absorption band centered at 364 nm upon the addition of Zn^{2+} could be explained on the basis of internal charge transfer (ICT) mechanism. The UV–vis spectra of **L2** showed three peaks at 285 nm, 346 nm and at 439 nm, while **L3** showed absorption peaks at 280 nm, 329 nm, and at 418 nm (Fig. 1, S2). UV–vis titrations of **L2**/**L3** (2×10^{-5} M) in a combination of DMF/Water (9:1) were performed with the gradual addition of Zn^{2+} to check the effects of Zn^{2+} on the absorption of **L2**/**L3** (Fig. 1,

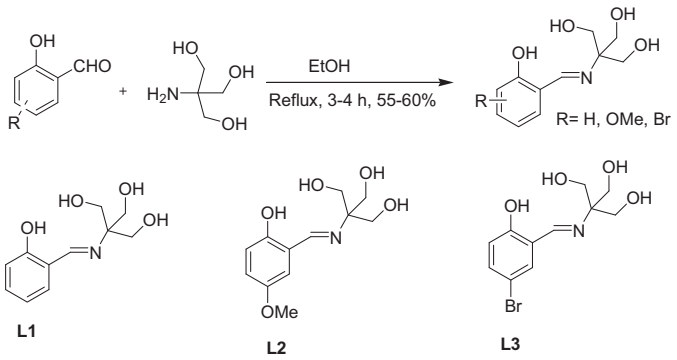

Scheme 1. Syntheses of **L1**, **L2** and **L3**.

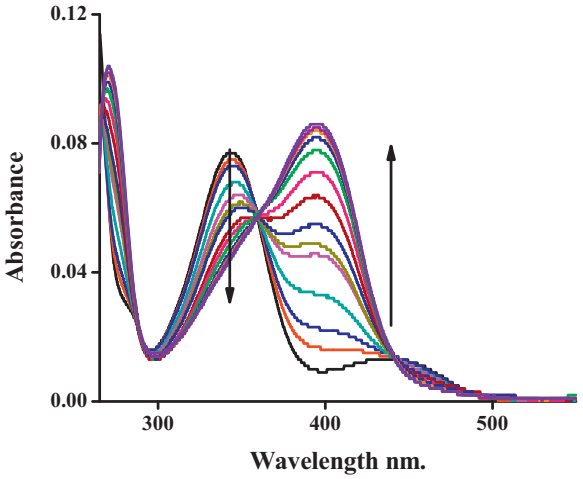

Fig. 1. UV–vis spectra of **L2** (2×10^{-5} M) in DMF/water (9:1, pH ~ 7.4) in the presence of various concentration of Zn^{2+} (0 μM, 5 μM, 10 μM, 15 μM, 20 μM, 25 μM, 30 μM, 35 μM, 40 μM, 80 μM, 120 μM, 160 μM, 200 μM, 240 μM). Upward arrow indicates gradual increase of absorption at 394 nm wavelength while downward arrow indicates gradual decrease in absorption at 346 nm wavelength with increasing concentration of externally added Zn^{2+}.

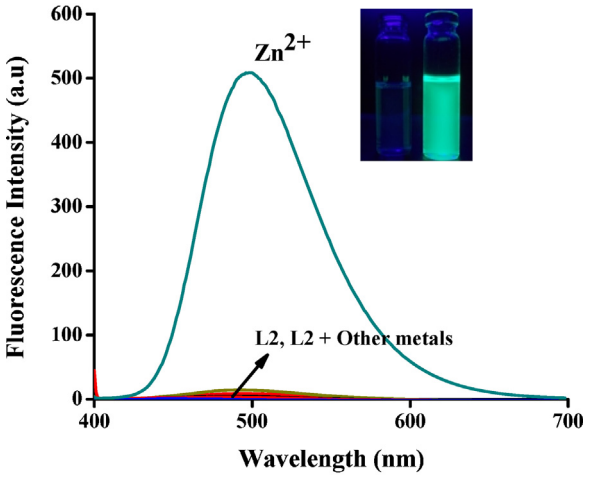

Fig. 2. Fluorescence spectra of **L2** (2×10^{-5} M) in DMF/water (9:1, pH ~ 7.4) in the presence of 240 μM of Zn^{2+} and in the presence of other metals like Li^+, Na^+, K^+, Ca^{2+}, Mg^{2+}, Mn^{2+}, Ba^{2+}, Cu^{2+}, Fe^{3+}, Cd^{2+}, Hg^{2+}, Ni^{2+}, Pb^{2+}, Sr^{2+}, Co^{2+}, Ag^+ (λ_{ex} = 394 nm).

S2). As expected, similar to that of **L1**, interaction of Zn^{2+} with **L2** and **L3** resulted in generation of new bands centered at 394 and at 377 nm, respectively.

From these absorption studies it was evident that all the three ligands **L1/L2/L3** formed stable complex with Zn^{2+} in the ground state. Next we investigated the effect of Zn^{2+} on the emission spectra of these three ligands. All the three ligands were found to be very weak fluorescent (quantum yield: 0.0024, 0.0025, 0.0027 for **L1**, **L2**, **L3**, respectively) with poor brightness (9.14, 10.93, 8.34 for **L1**, **L2**, **L3**, respectively). The weak fluorescence of these ligands was due to a combination of E/Z isomerization and ICT effect. When Zn^{2+} (16×10^{-5} M) was added to a solution of **L1** (2×10^{-5} M), a strong blue emission at 448 nm was observed when excited at 364 nm (quantum yield: 0.347 and brightness: 2.56×10^3) (Fig. S3). The addition of Zn^{2+} reduced the ICT effect and enhanced the structural rigidity by restricting the E/Z-isomerisation through complex formation resulting in activation of chelation enhanced fluorescence (CHEF) signaling. To test the effect of other mono-, di- and trivalent cations on the emission of **L1**, a broad spectrum of metal ions were investigated: Li^+, Na^+, K^+, Ca^{2+}, Mg^{2+}, Mn^{2+}, Fe^{3+}, Cu^{2+}, Zn^{2+}, Cd^{2+}, Co^{2+}, Sr^{2+}, Pb^{2+}, Ag^+, Ba^{2+}, Ni^{2+} and Hg^{2+} (Figs. S5 and S6). It was observed that CHEF signaling was completely Zn^{2+} specific as no other metal could induce any such fluorescence enhancement. The introduction of a methoxy functionality at the para position of OH group in **L2** resulted in 50 nm red shift, as compared to unsubstituted **L1**, in the emission band (λ_{em} = 499 nm) that was appeared upon interaction of **L2** with Zn^{2+} (λ_{ex} = 394 nm; quantum yield: 0.281 and brightness: 2.25×10^3) (Fig. 2). Though the interaction of

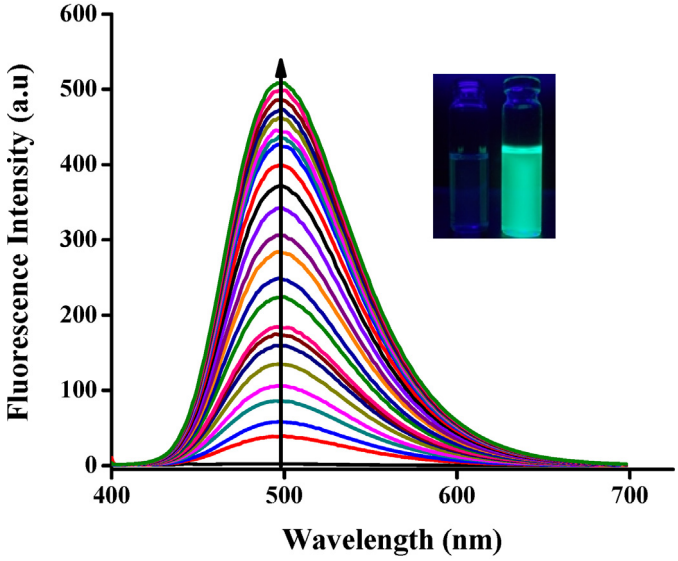

Fig. 4. Fluorescence spectra of **L2** (2×10^{-5} M) in DMF/water (9:1, pH ~ 7.4) in the presence of different concentrations of Zn^{2+} (0–240 μM) (λ_{ex} = 394 nm).

L2 with Zn^{2+} resulted in a glowing green emission, no such emission was observed in the presence of other mono-, di- and trivalent cations (Figs. 3 and 4).

L3, containing an electron withdrawing group at the para position of OH group, showed 6 nm red shift, as compared to unsubstituted **L1**, in the emission band when interacted with Zn^{2+} (λ_{ex} = 378 nm, λ_{em} = 454 nm, quantum yield: 0.117 and brightness:

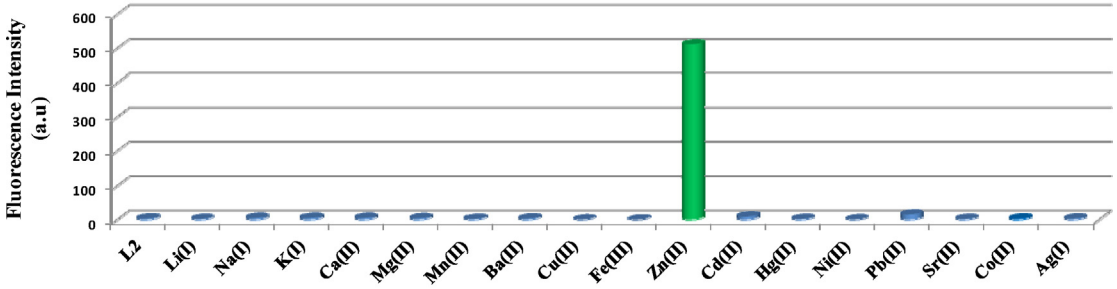

Fig. 3. Fluorescence intensity of **L2** (2×10^{-5} M) in DMF/water (9:1, pH ~ 7.4) in the presence of 240 μM of different types of metal ions as a bar graph.

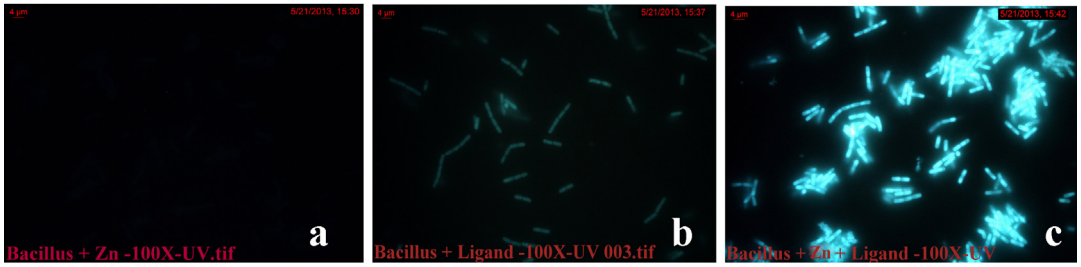

Fig. 5. Fluorescence Microscopic photographs of (a) *Bacillus thuringiensis* cells treated with Zn^{2+} (b) *B. thuringiensis* cells treated with **L2** (c) *B. thuringiensis* cells treated with Zn^{2+} followed by **L2**.

0.91×10^3) (Figs. S8 and S10). Similar to **L1** and **L2**, no other metal could induce such type of turn-on fluorescence signaling (Fig. S11). It is worth mentioning that in all the cases Zn^{2+} induced CHEF signaling was instant and stable up to minimum of 3 h confirming the potential of these probes for real-time analysis (Figs. S12–S14). All these three ligands showed efficient selective detection of Zn^{2+} in the presence of the most competitive bio-relevant metal ions Na^+, K^+, Ca^{2+} and Mg^{2+} (Figs. S15–S17). Moreover, **L1/L2/L3** did not show any fluorescence enhancement when interacted with Cd^{2+}/Pb^{2+} which is not the case for many literature reported turn-on Zn^{2+}-chemosensors. It is worth mentioning that **L2** can detect Zn^{2+} in the presence of higher percentage of water (50% water) though some extent of fluorescence quenching was observed in this condition (Fig. S18). The pH dependency studies proved that Zn^{2+}-induced fluorescence enhancement was observed in a pH range of 6.8–9.6 which is very much within thin the physiological pH range (Fig. S19). This encouraged us to check the efficiency of these ligands in fluorescence imaging of intracellular zinc.

Regarding stoichiometry of the formed complexes, Job's method [70] suggested 1:2 (metal:ligand) complex formation (Figs. S20 and S21). That **L1** formed 1:2 complex with Zn^{2+} was confirmed by the single crystal structure reported by Rao and co-workers [71]. Therefore, all these ligands prefer to form 1:2 (metal:ligand) complexes and this conclusion was supported by our theoretical studies (that has been explained in detail in later section). From the crystal structure it is evident that imine nitrogen, phenolic oxygen, and one of the alcoholic oxygens are the binding sites for Zn^{2+}.

3.3. ^1H NMR titrations

^1H NMR titration results clearly indicated the involvement of phenolic —OH, alcoholic —OH, and imine nitrogen in the 1:2 metal–ligand binding process. A downfield shift of 0.035 ppm was observed in case of the imine proton of **L2** whereas the phenolic proton peak almost disappeared (0.15 ppm upfield shifted) in the presence of Zn^{2+}. The three alcoholic protons peak at 4.68 ppm of **L2** got split into two peaks in the presence of Zn^{2+}, out of which one proton showed strong upfield shift (appeared at 5.84 ppm) indicating the involvement of this alcohol functionality in the complex formation (Fig. S22).

3.4. Detection limit and binding constant calculation

As one of the important criteria for a molecular probe to be an efficient bioimaging material is higher excitation/emission wavelengths [1], we selected **L2** as a model compound for biological studies. Limit of detection was calculated using (3σ/slope) method and we found that **L2** could detect as low as 20 nM of Zn^{2+} (Fig. S23) [72]. With the confirmation of 1:2 (metal:lignad) complex formation, the binding constant was calculated using Levenberg–Marquardt algorithm which showed high binding constant value $6.8 \times 10^9\ M^{-2}$ for **L2**-Zn^{2+} complex (Fig. S24).

3.5. Theoretical study

Density functional theory (DFT) calculations have been carried out to understand the complexation of Zn^{2+} with the TRIS based ligands and the observed spectral properties of ligands and zinc complexes. Theoretical analysis is focused on the structure and properties of **L2** and its Zn^{2+} complex (**L2**-Zn^{2+}) since all ligands (**L1**, **L2** and **L3**) and their Zn^{2+} complexes showed very similar spectral properties. All calculations were carried out at the M06-2X/6-311G(d,p) [73] level of DFT using Gaussian 09 suite of programs [74]. Optimized structures of **L2** and **L2-Zn^{2+}** complex (2:1) are given in Fig. S25. In **L2**, a weak H-bond interaction exists between the —OH group on phenyl ring and N (r(H—N) = 1.75 Å). **L2**-Zn^{2+} is a six coordinated complex formed by the coordination of Zn^{2+} with the lone pairs on two N atoms (Zn—N bond lengths are 2.07 and 2.08 Å), lone pairs on the oxygen atoms of two —OH groups (Zn—O bond lengths are 2.22 and 2.29 Å) and with two phenoxide anions (Zn—O bond distances are 2.02 and 1.99 Å).

Frontier molecular orbitals of both **L2** and **L2**-Zn^{2+} are calculated and are given in Fig. S26. The HOMO and HOMO-1 of **L2** are the π-orbitals of phenyl ring and lone pair orbitals on N and O atoms while LUMO and LUMO+1 are the corresponding π^*-orbitals. HOMO and HOMO-1 of **L2-Zn^{2+}** are nearly degenerate (energy difference between HOMO and HOMO-1 is 0.05 eV) and are formed by the π-orbitals of phenyl rings and the lone pair orbitals on N and O atoms while LUMOs are the π^*-orbitals on phenyl rings. The HOMO–LUMO energy gap in **L2** is 6.37 eV and the coordination of Zn^{2+} led to a decrease in the HOMO–LUMO energy gap to 5.68 eV. Molecular orbital analysis suggests that the peak at 344 nm in the UV–vis spectra of **L2** corresponds to the electronic excitation from HOMO to LUMO which gets diminished by the addition Zn^{2+}. The generation of a new peak at higher wavelength of 394 nm by the addition of Zn^{2+} can be attributed mainly to the HOMO to LUMO excitation in **L2**-Zn^{2+} with a minor contribution from HOMO-1 to LUMO transition. In **L2**-Zn^{2+} the first excited state (S1) gets more populated compared to **L2** since the electronic excitation takes place from HOMO and HOMO-1 [HOMO – (HOMO-1) = 0.05 eV] and the energy difference between LUMO and LUMO+1 is only 0.15 eV which might be a factor contributing to the fluorescent enhancement on the formation of **L2**-Zn^{2+}.

3.6. Biological studies

3.6.1. Living cell imaging (in vitro studies)

To investigate the potential of **L2** in intracellular zinc imaging, *B. thuringiensis* cells were treated with zinc salt first followed by **L2** and observed under a Leica DM 1000 Fluorescence microscope with UV filter. Strong green fluorescence was observed indicating the cell permeation and intracellular zinc-imaging capability of probe **L2** (Fig. 5). Cells treated with zinc salt only and with ligand only were chosen as control and no such strong green fluorescence was observed in any case.

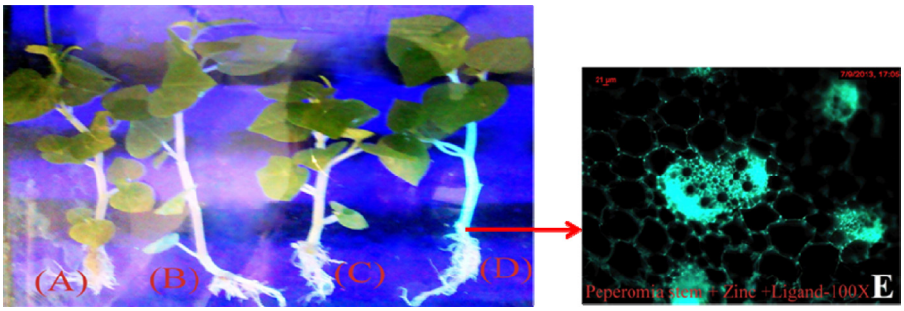

Fig. 6. Fluorescence micrograph of whole plant treated with (A) Zn^{2+}, (B) probe **L2**, (C) Zn^{2+} for 1 h, then with EDTA for another hour followed by **L2** for 1 h, (D) Zn^{2+} for 1 h followed by **L2** for 1 h, and (E) transverse section of *Peperomia pellucida*, treated with Zn^{2+} for 1 h followed by **L2** for 1 h (fluorescing vascular bundle observed under fluorescence microscope).

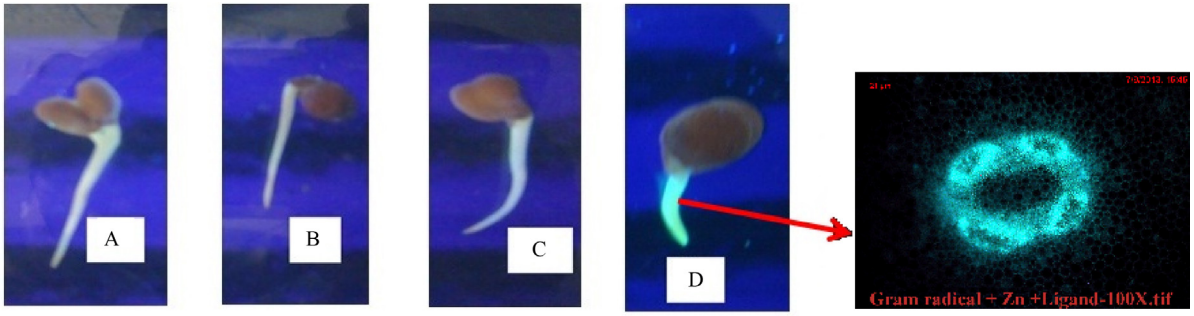

Fig. 7. Fluorescence micrograph of Gram radicals after treatment with (A) Zn^{2+} for 1 h, (B) **L2** for 1 h, (C) Zn^{2+} for an hour, then with EDTA for another hour followed by treatment with **L2** for 1 h, (D) Zn^{2+} for 1 h followed by **L2** for another 1 h, and (E) transverse section of seed radicals treated with Zn^{2+} for 1 h followed by **L2** for 1 h (fluorescing vascular bundle observed under fluorescence microscope).

3.6.2. *Fluorescence in vivo imaging of Zn^{2+} in a whole-plant*

Peperomia pellucida, family Piperomiacea, a small herbaceous plant with transparent stem was used in this experiment for tracking/imaging translocation of zinc through stem with the help of ligand **L2** as a fluorescent bioimaging probe. To perform this experiment, freshly collected plants were thoroughly washed to remove soil and darts. Then the roots of the plant were dipped into $Zn(NO_3)_2{\cdot}6H_2O$ solution. After 1 h, the dipped portion of the plant was washed several times to remove externally bound zinc, if any, and again dipped the root portion into a solution of **L2** (0.5 mM). During treatment of the plant with ligand, and in order to avoid photobleaching of **L2**, the tube containing the probe solution was covered carefully with a black paper leaving the top portion of the tube open in such a way that only the top portion of the plant got exposed to sunlight to ensure transpirational loss of water resulting in efficient sucking of **L2** through root. The fluorescence imaging helped us in knowing the movement of the probe **L2** through the various parts of the plant as the complexation between **L2** and Zn^{2+} resulted in strong emission (Fig. 6). This experiment clearly demonstrated possibility of using **L2** for fluorescence imaging of zinc *in vivo*. As *in vivo* imaging experiments using animal models are always expensive and time consuming, this work may help in screening *in vivo* imaging potential of a probe, particularly its stability and real-time analysis possibility inside living systems, before being tested on animals.

3.6.3. *In vivo zinc-imaging in gram sprouts*

As an essential micronutrient, zinc is need for the normal growth of plant, animal and human [75,76]. Due to high consumption of cereal crops in developing countries, the zinc-enriched cereal crops could partially compensate zinc deficiency in human body [77]. Concentration of soil–zinc pools is the key in enriching cereal crops with zinc. This has been investigated and documented that during seed germination, zinc-mobilization occurs from seed to the sprout. Therefore, the detection and localization of zinc in seed sprouts may enable us to know about the zinc enrichment of that particular kind of seed. We became interested to check the potential of probe **L2** in *in vivo* imaging of zinc present in gram seed sprouts. We observed that the present probe **L2** successfully imaged the Zn^{2+} present in the sprouts with a strong green emission proving further the cell permeability and *in vivo* bioimaging capabilities of probe **L2** (Fig. 7). To prove this further, when the zinc treated sprouts were treated further with strong chelating agent EDTA followed by **L2**, no imagining was observed (Fig. 4C). As the intensity of the emission is purely zinc-concentration dependent, **L2** can be used as an indicator to investigate the efficiency of various strategies used for zinc enrichment in cereal crops.

4. Conclusion

To summarize, TRIS-based three molecular probes **L1**/**L2**/**L3** were utilized for the turn-on detection of zinc at nanomolar level. The fluorescence enhancement could be explained on the basis of CHEF signaling and ICT mechanism. As during photophysical studies it was revealed that **L2** has higher excitation/emission wavelengths, it was chosen for biological studies. The potential of **L2** as an efficient fluorescence bioimaging material, both *in vitro* and *in vivo*, was tested both in plant system and in living organisms. While *in vitro* studies on intracellular zinc imaging confirmed the cell permeation capability of **L2**, the imaging of zinc in a whole plant supported *in vivo* imaging potential of **L2** in real-time. In another *in vivo* study, **L2** successfully imaged the zinc-pool of gram sprouts establishing its efficiency as a molecular marker for the bioimaging of zinc present in seeds. We trust that the longer stability of fluorescence emission of **L2**-Zn^{2+} ensemble, more than 3 h, and its nanomolar zinc detection capability will make **L2** as a potential probe for staining zinc in biological systems.

Acknowledgements

The work was funded by the Department of Science and Technology, India (Grant No. SERB/F/2408/2012-13). SS is grateful to IIT Mandi for his fellowship. We thankfully acknowledge the Director, IIT Mandi for research facilities. Advanced Materials Research Center (AMRC), IIT Mandi, is thankfully acknowledged for sophisticated instrument facility support. We also gratefully acknowledge the support of USIC (Burdwan University) for fluorescence microscope facility. We are thankful to the reviewers for their valuable comments.

Appendix A. Supplementary data

Supplementary data associated with this article can be found, in the online version, at http://dx.doi.org/10.1016/j.jphotochem.2013.12.012.

References

[1] Z. Xu, J. Yoon, D.R. Spring, Fluorescent chemosensors for Zn^{2+}, Chem. Soc. Rev. 39 (2010) 1996–2006.
[2] T. Terai, T. Nagano, Small-molecule fluorophores and fluorescent probes for bioimaging, Pflug. Arch.: Eur. J. Phys. 465 (2013) 347–359.
[3] K. Kikuchi, K. Komatsu, T. Nagano, Zinc sensing for cellular application, Curr. Opin. Chem. Biol. 8 (2004) 182–191.
[4] E.M. Nolan, S.J. Lippard, Small-molecule fluorescent sensors for investigating zinc metalloneurochemistry, Acc. Chem. Res. 42 (2009) 193–203.
[5] D.W. Domaille, E.L. Que, C.J. Chang, Synthetic fluorescent sensors for studying the cell biology of metals, Nat. Chem. Biol. 4 (2008) 168–175.
[6] Y. Yang, Q. Zhao, W. Feng, F. Li, Luminescent chemodosimeters for bioimaging, Chem. Rev. 113 (2013) 192–270.
[7] H. Komatsu, T. Miki, D. Citterio, T. Kubota, Y. Shindo, Y. Kitamura, K. Oka, K. Suzuki, Single molecular multianalyte (Ca^{2+}, Mg^{2+}) fluorescent probe and applications to bioimaging, J. Am. Chem. Soc. 127 (2005) 10798–10799.
[8] R.P. Haugland, Handbook of Fluorescent Probes and Research Chemicals, 9th ed., Molecular Probes, Eugene, OR, 2002.
[9] N.C. Lim, H.C. Freake, C. Brückner, Illuminating zinc in biological systems, Chem. Eur. J. 11 (2005) 38–49.
[10] Z. Huang, S.J. Lippard, P.M. Conn, Chapter twenty-three – illuminating mobile zinc with fluorescence: from cuvettes to live cells and tissues, in: Methods in Enzymology, Academic Press, 2012, pp. 445–468.
[11] S.K. Ghosh, P. Kim, X.-a. Zhang, S.-H. Yun, A. Moore, S.J. Lippard, Z. Medarova, A novel imaging approach for early detection of prostate cancer based on endogenous zinc sensing, Cancer Res. 70 (2010) 6119–6127.
[12] H. Kitano, Systems biology: a brief overview, Science 295 (2002) 1662–1664.
[13] L.D. Lavis, T.-Y. Chao, R.T. Raines, Fluorogenic label for biomolecular imaging, ACS Chem. Biol. 1 (2006) 252–260.
[14] G. Sivaraman, V. Sathiyaraja, D. Chellappa, Turn-on fluorogenic and chromogenic detection of Fe(III) and its application in living cell imaging, J. Lumin. 145 (2014) 480–485.
[15] G. Sivaraman, T. Anand, D. Chellappa, Quick accessible dual mode turn-on red fluorescent chemosensor for Cu(ii) and its applicability in live cell imaging, RSC Adv. 3 (2013) 17029–17033.
[16] G. Sivaraman, D. Chellappa, Rhodamine based sensor for naked-eye detection and live cell imaging of fluoride ions, J. Mater. Chem. B 1 (2013) 5768–5772.
[17] S. Kim, J.Y. Noh, K.Y. Kim, J.H. Kim, H.K. Kang, S.-W. Nam, S.H. Kim, S. Park, C. Kim, J. Kim, Salicylimine-based fluorescent chemosensor for aluminum ions and application to bioimaging, Inorg. Chem. 51 (2012) 3597–3602.
[18] L. Fan, Y.-J. Fu, Q.-L. Liu, D.-T. Lu, C. Dong, S.-M. Shuang, Novel far-visible and near-infrared pH probes based on styrylcyanine for imaging intracellular pH in live cells, Chem. Commun. 48 (2012) 11202–11204.
[19] J. Xie, Y. Chen, W. Yang, D. Xu, K. Zhang, Water soluble 1,8-naphthalimide fluorescent pH probes and their application to bioimagings, J. Photochem. Photobiol. A: Chem. 223 (2011) 111–118.
[20] J.Y. Noh, S. Kim, I.H. Hwang, G.Y. Lee, J. Kang, S.H. Kim, J. Min, S. Park, C. Kim, J. Kim, Solvent-dependent selective fluorescence assay of aluminum and gallium ions using julolidine-based probe, Dyes Pigments 99 (2013) 1016–1021.
[21] A.K. Mahapatra, J. Roy, S.K. Manna, S. Kundu, P. Sahoo, S.K. Mukhopadhyay, A. Banik, Hg^{2+}-selective "turn-on" fluorescent chemodosimeter derived from glycine and living cell imaging, J. Photochem. Photobiol. A: Chem. 240 (2012) 26–32.
[22] W. Maret, Zinc biochemistry, physiology, and homeostasis. Recent insights and current trends, Biometals 14 (2001) 187–190.
[23] X. Zhou, F. Su, Y. Tian, C. Youngbull, R.H. Johnson, D.R. Meldrum, A new highly selective fluorescent K+ sensor, J. Am. Chem. Soc. 133 (2011) 18530–18533.
[24] Z.-Q. Hu, Y.-C. Feng, H.-Q. Huang, L. Ding, X.-M. Wang, C.-S. Lin, M. Li, C.-P. Ma, Fe^{3+}-selective fluorescent probe based on rhodamine B and its application in bioimaging, Sens. Actuators B 156 (2011) 428–432.
[25] L. Qu, C. Yin, F. Huo, Y. Zhang, Y. Li, A commercially available fluorescence chemosensor for copper ion and its application in bioimaging, Sens. Actuators B 183 (2013) 636–640.
[26] V. Chandrasekhar, S. Das, R. Yadav, S. Hossain, R. Parihar, G. Subramaniam, P. Sen, Novel chemosensor for the visual detection of copper(II) in aqueous solution at the ppm level, Inorg. Chem. 51 (2012) 8664–8666.
[27] G.C. Midya, S. Paladhi, S. Bhowmik, S. Saha, J. Dash, Design and synthesis of an on-off click fluorophore that executes a logic operation and detects heavy and transition metal ions in water and living cells, Org. Biomol. Chem. 11 (2013) 3057–3063.
[28] M.P. Cuajungco, G.J. Lees, Zinc metabolism in the brain: relevance to human neurodegenerative disorders, Neurobiol. Dis. 4 (1997) 137–169.
[29] D.W. Choi, J.Y. Koh, Zinc and brain injury, Annu. Rev. Neurosci. 21 (1998) 347–375.
[30] P.D. Zalewski, I.J. Forbes, W.H. Betts, Correlation of apoptosis with change in intracellular labile Zn(II) using zinquin [(2-methyl-8-p-toluenesulphonamido-6-quinolyloxy)acetic acid], a new specific fluorescent probe for Zn(II), Biochem. J. 296 (1993) 400–403.
[31] K. Falchuk, The molecular basis for the role of zinc in developmental biology, Mol. Cell. Biochem. 188 (1998) 41–48.
[32] B.L. Vallee, K.H. Falchuk, The biochemical basis of zinc physiology, Physiol. Rev. 73 (1993) 79–118.
[33] W. Maret, C. Jacob, B.L. Vallee, E.H. Fischer, Inhibitory sites in enzymes: zinc removal and reactivation by thionein, Proc. Natl. Acad. Sci. U.S.A. 96 (1999) 1936–1940.
[34] E. Kimura, T. Koike, Recent development of zinc-fluorophores, Chem. Soc. Rev. 27 (1998) 179–184.
[35] S.J. Lippard, J.M. Berg, Principles of Bioinorganic Chemistry, University Science Books, Mill Valley, CA, 1994.
[36] S.C. Burdette, G.K. Walkup, B. Spingler, R.Y. Tsien, S.J. Lippard, Fluorescent sensors for Zn^{2+} based on a fluorescein platform: synthesis, properties and intracellular distribution, J. Am. Chem. Soc. 123 (2001) 7831–7841.
[37] T. Hirano, K. Kikuchi, Y. Urano, T. Nagano, Improvement and biological applications of fluorescent probes for zinc, ZnAFs, J. Am. Chem. Soc. 124 (2002) 6555–6562.
[38] S.L. Sensi, D. Ton-That, P.G. Sullivan, E.A. Jonas, K.R. Gee, L.K. Kaczmarek, J.H. Weiss, Modulation of mitochondrial function by endogenous Zn^{2+} pools, Proc. Natl. Acad. Sci. U.S.A. 100 (2003) 6157–6162.
[39] K.R. Gee, Z.-L. Zhou, W.-J. Qian, R. Kennedy, Detection and imaging of zinc secretion from pancreatic $\hat{I}^2$-cells using a new fluorescent zinc indicator, J. Am. Chem. Soc. 124 (2002) 776–778.
[40] K.R. Gee, Z.L. Zhou, D. Ton-That, S.L. Sensi, J.H. Weiss, Measuring zinc in living cells: a new generation of sensitive and selective fluorescent probes, Cell Calcium 31 (2002) 245–251.
[41] S.L. Sensi, D. Ton-That, J.H. Weiss, A. Rothe, K.R. Gee, A new mitochondrial fluorescent zinc sensor, Cell Calcium 34 (2003) 281–284.
[42] W.-J. Qian, K.R. Gee, R.T. Kennedy, Imaging of Zn^{2+} release from pancreatic $\hat{I}^2$-cells at the level of single exocytotic events, Anal. Chem. 75 (2003) 3468–3475.
[43] P.D. Zalewski, I.J. Forbes, R.F. Seamark, R. Borlinghaus, W.H. Betts, S.F. Lincoln, A.D. Ward, Flux of intracellular labile zinc during apoptosis (gene-directed cell death) revealed by a specific chemical probe, Zinquin, Chem. Biol. 1 (1994) 153–161.
[44] T. Hirano, K. Kikuchi, Y. Urano, T. Higuchi, T. Nagano, Novel zinc fluorescent probes excitable with visible light for biological applications, Angew. Chem. Int. Ed. 39 (2000) 1052–1054.
[45] S.C. Burdette, C.J. Frederickson, W. Bu, S.J. Lippard, ZP4, an improved neuronal Zn^{2+} sensor of the zinpyr family, J. Am. Chem. Soc. 125 (2003) 1778–1787.
[46] S. Maruyama, K. Kikuchi, T. Hirano, Y. Urano, T. Nagano, A. Novel, Cell-permeable, fluorescent probe for ratiometric imaging of zinc ion, J. Am. Chem. Soc. 124 (2002) 10650–10651.
[47] E.M. Nolan, J. Jaworski, K.-I. Okamoto, Y. Hayashi, M. Sheng, S.J. Lippard, QZ1 and QZ2: rapid, reversible quinoline-derivatized fluoresceins for sensing biological Zn(II), J. Am. Chem. Soc. 127 (2005) 16812–16823.
[48] C.C. Woodroofe, R. Masalha, K.R. Barnes, C.J. Frederickson, S.J. Lippard, Membrane-permeable and -impermeable sensors of the zinpyr family and their application to imaging of hippocampal zinc in vivo, Chem. Biol. 11 (2004) 1659–1666.
[49] C.J. Chang, E.M. Nolan, J. Jaworski, S.C. Burdette, M. Sheng, S.J. Lippard, Bright fluorescent chemosensor platforms for imaging endogenous pools of neuronal zinc, Chem. Biol. 11 (2004) 203–210.
[50] S. Lee, J.H. Lee, T. Pradhan, C.S. Lim, B.R. Cho, S. Bhuniya, S. Kim, J.S. Kim, Fluorescent turn-on Zn^{2+} sensing in aqueous and cellular media, Sens. Actuators B 160 (2011) 1489–1493.
[51] Y. Ding, Y. Xie, X. Li, J.P. Hill, W. Zhang, W. Zhu, Selective and sensitive turn-on fluorescent Zn^{2+} sensors based on di- and tripyrrins with readily modulated emission wavelengths, Chem. Commun. 47 (2011) 5431–5433.
[52] S. Iyoshi, M. Taki, Y. Yamamoto, Development of a cholesterol-conjugated fluorescent sensor for site-specific detection of zinc ion at the plasma membrane, Org. Lett. 13 (2011) 4558–4561.
[53] P. Jiang, Z. Guo, Fluorescent detection of zinc in biological systems: recent development on the design of chemosensors and biosensors, Coord. Chem. Rev. 248 (2004) 205–229.
[54] J.H. Kim, I.H. Hwang, S.P. Jang, J. Kang, S. Kim, I. Noh, Y. Kim, C. Kim, R.G. Harrison, Zinc sensors with lower binding affinities for cellular imaging, Dalton Trans. 42 (2013) 5500–5507.

[55] M. Kumar, N. Kumar, V. Bhalla, A naphthalimide based chemosensor for Zn^{2+}, pyrophosphate and H_2O_2: sequential logic operations at the molecular level, Chem. Commun. 49 (2013) 877–879.
[56] Z. Liu, C. Zhang, Y. Chen, W. He, Z. Guo, An excitation ratiometric Zn^{2+} sensor with mitochondria-targetability for monitoring of mitochondrial Zn^{2+} release upon different stimulations, Chem. Commun. 48 (2012) 8365–8367.
[57] X.-B. Yang, B.-X. Yang, J.-F. Ge, Y.-J. Xu, Q.-F. Xu, J. Liang, J.-M. Lu, Benzo[a]phenoxazinium-based red-emitting chemosensor for zinc ions in biological media, Org. Lett. 13 (2011) 2710–2713.
[58] Q.-H. You, P.-S. Chan, W.-H. Chan, S.C.K. Hau, A.W.M. Lee, N.K. Mak, T.C.W. Mak, R.N.S. Wong, A quinolinyl antipyrine based fluorescence sensor for Zn^{2+} and its application in bioimaging, RSC Adv. 2 (2012) 11078–11083.
[59] Z. Zhang, F.-W. Wang, S.-Q. Wang, F. Ge, B.-X. Zhao, J.-Y. Miao, A highly sensitive fluorescent probe based on simple pyrazoline for Zn^{2+} in living neuron cells, Org. Biomol. Chem. 10 (2012) 8640–8644.
[60] Y. Zhou, Z.-X. Li, S.-Q. Zang, Y.-Y. Zhu, H.-Y. Zhang, H.-W. Hou, T.C.W. Mak, A novel sensitive turn-on fluorescent Zn^{2+} chemosensor based on an easy to prepare C3-symmetric Schiff-base derivative in 100% aqueous solution, Org. Lett. 14 (2012) 1214–1217.
[61] P. Du, S.J. Lippard, A highly selective turn-on colorimetric, red fluorescent sensor for detecting mobile zinc in living cells, Inorg. Chem. 49 (2010) 10753–10755.
[62] E.M. Nolan, J.W. Ryu, J. Jaworski, R.P. Feazell, M. Sheng, S.J. Lippard, Zinspy sensors with enhanced dynamic range for imaging neuronal cell zinc uptake and mobilization, J. Am. Chem. Soc. 128 (2006) 15517–15528.
[63] M. Iniya, D. Jeyanthi, K. Krishnaveni, A. Mahesh, D. Chellappa, Triazole based ratiometric fluorescent probe for Zn^{2+} and its application in bioimaging, Spectrochim. Acta A (2013), http://dx.doi.org/10.1016/j.saa.2013.09.107.
[64] G. Sivaraman, T. Anand, D. Chellappa, Turn-on fluorescent chemosensor for Zn(II) via ring opening of rhodamine spirolactam and their live cell imaging, Analyst 137 (2012) 5881–5884.
[65] S. Zhu, J. Zhang, J. Janjanam, G. Vegesna, F.-T. Luo, A. Tiwari, H. Liu, Highly water-soluble BODIPY-based fluorescent probes for sensitive fluorescent sensing of zinc(ii), J. Mater. Chem. B 1 (2013) 1722–1728.
[66] M.V. Alfimov, A.V. Churakov, Y.V. Fedorov, O.A. Fedorova, S.P. Gromov, R.E. Hester, J.A.K. Howard, L.G. Kuz'mina, I.K. Lednev, J.N. Moore, Structure and ion-complexing properties of an aza-15-crown-5 ether dye: synthesis, crystallography, NMR spectroscopy, spectrophotometry and potentiometry, J. Chem. Soc., Perkin Trans. 2 (1997) 2249–2256.
[67] Y. Kubo, M. Kato, Y. Misawa, S. Tokita, A fluorescence-active 1,3-bis(isothiouronium)-derived naphthalene exhibiting versatile binding modes toward oxoanions in aqueous MeCN solution: new methodology for sensing oxoanions, Tetrahedron Lett. 45 (2004) 3769–3773.
[68] R.F. Martínez, M. Ávalos, R. Babiano, P. Cintas, J.L. Jiménez, M.E. Light, J.C. Palacios, Schiff bases from TRIS and ortho-hydroxyarenecarbaldehydes: structures and tautomeric equilibria in the solid state and in solution, Eur. J. Org. Chem. (2011) 3137–3145.
[69] Y. Sui, X. Zeng, X. Fang, X. Fu, Y.a. Xiao, L. Chen, M. Li, S. Cheng, Syntheses, structure, redox and catalytic epoxidation properties of dioxomolybdenum(VI) complexes with Schiff base ligands derived from tris(hydroxymethyl)amino methane, J. Mol. Catal. A: Chem. 270 (2007) 61–67.
[70] P. Job, Ann. Chim. Applicata 9 (1928) 113–203.
[71] M. Dey, P. Chebrolu, P. Rao, K. Saarenketo, E. Rissanen, Kolehmainen, Four-, five- and six-coordinated Zn(II) complexes of OH-containing ligands: syntheses, structure and reactivity, Eur. J. Inorg. Chem. (2002) 2207–2215.
[72] G.L. Long, J.D. Winefordner, Limit of detection a closer look at the IUPAC definition, Anal. Chem. 55 (1983) 712A–724A.
[73] Y. Zhao, D. Truhlar, The M06 suite of density functionals for main group thermochemistry, thermochemical kinetics, noncovalent interactions, excited states, and transition elements: two new functionals and systematic testing of four M06-class functionals and 12 other functionals, Theor. Chem. Acc. 120 (2008) 215–241.
[74] M.J. Frisch, et al., Gaussian 09, Revision-C.01, Gaussian, Inc., Wallingford, CT, 2010.
[75] S.R. Fard, A. Khourgami, M. Rafee, H. Nasrollahi, Ann. Biol. Res. 3 (2012) 4166–4171.
[76] I. Cakmak, Enrichment of cereal grains with zinc: agronomic or genetic biofortification? Plant Soil 302 (2008) 1–17.
[77] L. Ozturk, M.A. Yazici, C. Yucel, A. Torun, C. Cekic, A. Bagci, H. Ozkan, H.-J. Braun, Z. Sayers, I. Cakmak, Physiol. Plant. 128 (2008) 144–152.